Theoretical and Experimental Investigation of Explosion Characteristics of Hydrogen Explosion in a Closed Vessel

Huadao Xing [1,2,*], **Runze Yu** [3], **Guangan Xu** [3], **Xiaodong Li** [1], **Yanyu Qiu** [3,*], **Derong Wang** [3], **Bin Li** [2] **and Lifeng Xie** [2]

1   School of Mechanical Engineering, Nanjing University of Science and Technology, Nanjing 210094, China
2   School of Chemical Engineering, Nanjing University of Science and Technology, Nanjing 210094, China
3   State Key Laboratory for Disaster Prevention & Mitigation of Explosion & Impact, The Army Engineering University of PLA, Nanjing 210007, China
*   Correspondence: xinghuadao2000@163.com (H.X.); qiuyanyu78@sina.com (Y.Q.)

Abstract: A simplified model that calculates the deflagration pressure–time curves of a hydrogen explosion was proposed. The deflagration parameters (pressure peak, duration, deflagration index, and impulse) of hydrogen–air mixtures with different hydrogen concentrations were experimentally investigated. The results show that the pressure curves calculated by the model are consistent with experimental data pertaining to a methane and hydrogen explosion. By comparison, the pressure peak and deflagration index are found to be influenced by the aspect ratio and surface area of vessels. The impulse and explosion times at fuel-lean hydrogen concentrations are greater than those at fuel-rich concentrations. When the hydrogen concentration is between 34 vol.% and 18 vol.%, the greatest explosion damage effect is formed by both the overpressure and the impulse, which should be considered for hydrogen explosion safety design in industrial production.

Keywords: pressure profile; impulse; hydrogen concentration; distributed calculation model

1. Introduction

Hydrocarbon fuel combustion yields huge amounts of greenhouse gases, resulting in an increase in global warming and environmental pollution. Hydrogen, regarded as a clean carrier of energy for transport and energy applications [1], is widely applied in internal combustion engines, aerospace applications, fuel cells, rocket propulsion, and industrial production [2–5]. However, hydrogen has a broad range of explosion, low ignition energy, diffusivity, and reactivity, causing combustion and even explosion accidents that can cause explosion hazards and structural failure [6–8]. Therefore, hydrogen explosion characteristics should be considered in engineering design and application, hence meeting the need for a reference for risk assessment and the design of explosion venting systems.

With reference to the characteristics of a hydrogen explosion, many scholars have conducted numerous theoretical and experimental studies [9,10]. Bradley and Mitcheson [11] promoted three mathematical solutions as models for gas explosions in a closed spherical vessel. Jo and Crowl [12] constructed a flame growth model to predict the flame front propagation, and validated the pressure–time curves calculated by the experimental data for hydrogen and methane obtained in a 20 L spherical vessel. Walsh et al. [13] established a thermodynamic model using the conservation of mass and energy, which considers the temperature-dependent specific heats for both the reactants and products. Rota et al. [14] developed a detailed model based on conservation laws and physico–chemical relationships [15]. The result showed that the error of the maximum pressure peaks obtained by experimental and theoretical data is equal to 10%. For the experiment, Thomas and Oakley [16] investigated the explosion pressure of a hydrogen–air mixture using experimental studies and theoretical predictions. Dahoe [17] explored the explosion parameters of hydrogen–air mixtures in a 169 mL cylindrical vessel. The results showed that the

internal pressure first increases and then decreases with time. Sun et al. [18–20] revealed the propagation mechanism of a detonation wave in a duct, and discussed the effect of obstacle size on the mechanism of the transmission of a detonation wave, and presented the critical conditions for detonation [21]. The effects of the hydrogen concentration on the flame propagation speed and explosion pressure in a spherical vessel were investigated by Cao et al. [22], and the result indicated that the maximum length of the flame increases with the hydrogen concentration. Cao et al. [23] estimated the effect of the hydrogen fraction on jet flame propagation characteristics using experimental and simulation methods. They found that secondary combustion occurs with a high hydrogen fraction, and the variations of the pressure wave and pressure oscillations obtained by experiment and simulation are consistent. In addition, the deflagration index (K_G) is also a key characteristic parameter in such hazard evaluation [24–27], which is calculated using the following Equation based on a cube-root law.

$$K_G = (dP/dt)_{max} \sqrt[3]{V_0} \tag{1}$$

where V_0 is the vessel volume. Some studies on K_G have been reported in the existing literature. Razus et al. [28] claimed that K_G increases with increasing vessel volume, and the explosion hazard is more severe for higher K_G values [29]. Sun and Li [30] found that when the equivalent ratio is equal to 1.4, the flame propagation speed and the value of $(dP/dt)_{max}$ are the greatest, and the duration of the explosion is the shortest [31].

From the above review, the previous work on hydrogen explosion behavior has mainly focused on the pressure, flame propagation, and K_G. Little research focuses on the effects of the impulse on the damage to personnel and structures caused by a hydrogen explosion. The key parameters of overpressure and impulse are mainly responsible for personal injury and door and window component destruction [32]. Li and Hao [33] investigated the internal and external pressure and impulse from vented gas explosions in large cylindrical tanks by comparing the experiment and numerical simulation, and found that venting size, tank diameter, and tank height have significant effects on the pressure and impulse in an adjacent tank. Ferradás et al. [34] studied the characteristic overpressure–impulse–distance to determine the damage to humans from bursting spherical vessels. Table 1 summarizes the damage corresponding to different overpressures and impulses [35,36].

Table 1. Pressure and impulse corresponding to the severity of damage [35,36].

	Effect		Overpressure (MPa)	I (MPa·s)
Humans	Eardrum rupture	Threshold	0.0345	-
		50%	0.103–0.138	-
	Lung damage	Threshold	0.083–0.103	0.0166–0.021
		Severe	0.255	0.051
	Lethality (lung hemorrhage)	Threshold	0.255–0.359	0.051–0.072
		50%	0.359–0.497	0.072–0.099
		100%	0.497–0.69	0.099–0.138
Buildings	Partially demolished	80%	0.035	0.013
	Moderated damage	25%	0.028	0.011
	Minor damage (repairable)	10%	0.012	0.006

In summary, a simplified model for predicting the pressure profiles of hydrogen explosion was developed based on flame surface, and the distribution calculation method was employed to simplify the explosion parameters. Meanwhile, explosion experiments of hydrogen–air mixtures were conducted in a cylindrical vessel; by changing the hydrogen concentration, the explosion parameters (overpressure, pressure rise rate, and impulse) of hydrogen–air mixtures in the closed vessel were investigated. The results can provide theoretical guidelines for the design of explosion venting systems and safety protection in practice.

2. Theoretical Model

The existing calculation models of the pressure curves depend on the solution of partial differential equations involving the rate of pressure increase, leading to a complex solution process. In the present work, the combustion process was analyzed by differentiating the deflagration process, which can be divided into three stages (burned, burning, and unburned) in each period. The combustion process can be adopted to predict the pressure–time curves and the flame radius. The result can provide a reference for rapid evaluation of an internal explosion in engineering practice.

Basic Assumption

The flame propagation in a closed spherical vessel was studied and established in the current section based on the following assumptions: (1) the unburned gas is isentropically compressed; (2) both unburned and burned gas are in an ideal state; (3) the buoyancy effects are negligible; (4) the gas is uniformly distributed. The relative parameters and states of the combustion propagation process are shown in Figure 1. States (a) and (b) in Figure 1 assume that the flammable gas is burned at constant pressure. In states (b) and (c), the increase in the radius of burned gas assumes an adiabatic constant-volume process.
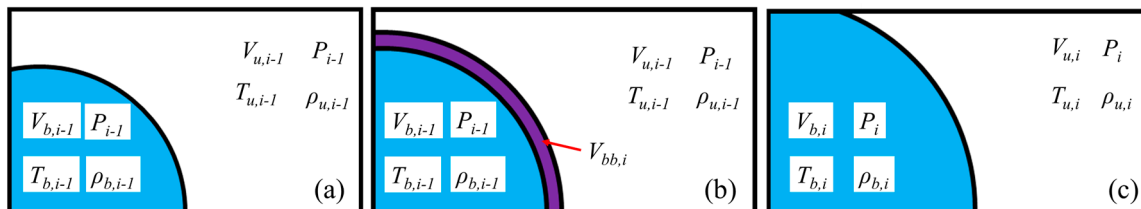

Figure 1. Diagrammatic representation of the combustion process.

The pressure was calculated using the following equation:

$$P_i = P_{i-1} + \Delta\mu_i(P_{\max} - P_0) \tag{2}$$

where P_i and P_{i-1} are the internal pressure in time i and $i-1$, respectively; $P_{\max}$ denotes the maximum explosion pressure; P_0 is the initial pressure; $\Delta\mu_i$ represents burnout rate in time Δt_i, which is defined as the mass of gas burned in time Δt_i divided by the total mass, as follows:

$$\Delta\mu_i = V_{\mathrm{bb},i}\rho_{\mathrm{u},i-1}/(V_0\rho_0) \tag{3}$$

where $V_{\mathrm{bb},i}$ denotes the volume of gas burned in time i; $\rho_{\mathrm{u},i-1}$ is the unburned gas density in time $i-1$; V_0 is the container volume; ρ_0 is the initial density.

The following correlation for adiabatic compression is presented. Therefore, we have:

$$\rho_{\mathrm{u},i-1}/\rho_0 = \sqrt[\gamma_u]{P_{i-1}/P_0} \tag{4}$$

where γ_u is the adiabatic index of hydrogen and air mixtures.

Substituting Equation (4) into Equation (3) yields the following expression for burnout rate:

$$\Delta\mu_i = (V_{\mathrm{bb},i}/V_0)\sqrt[\gamma_u]{P_{i-1}/P_0} \tag{5}$$

Assuming the flame spreads in a spherical front, the expression of $V_{\mathrm{bb},i}$ is:

$$V_{\mathrm{bb},i} = (4\pi/3)\left(\sqrt[3]{3V_{\mathrm{b},i-1}/(4\pi)} + S\Delta t\right)^3 - V_{\mathrm{b},i-1} \tag{6}$$

where $V_{\mathrm{b},i-1}$ is the volume of gas burned at time $i-1$ and S denotes the laminar flame velocity. According to an assumption of isentropic compression, the laminar burning velocity

is correlated with the initial temperature and pressure in a power–law relationship [37]. The following relationship thus holds [38,39]:

$$S = S_L \left(\frac{T}{T_0} \right)^m \cdot \left(\frac{P}{P_0} \right)^n \tag{7}$$

where S_L is the laminar burning velocity at initial T_0 and P_0; m and n are the temperature index and pressure index, respectively. Values of m, n, and S_L for hydrogen–air mixtures at various equivalence ratios (Φ) can be determined according to the literature [40].

$$m = 1.54 + 0.026(\Phi - 1) \tag{8}$$

$$n = 0.43 + 0.003(\Phi - 1) \tag{9}$$

Then, according to the isentropic compression equation, the $V_{u,i}$ and $V_{b,i}$ are the volume of unburned gas and burned gas at time i, which are calculated by the following expressions, respectively.

$$\rho_{u,i}/\rho_0 = \sqrt[\gamma_u]{P_i/P_0} \tag{10}$$

$$T_{u,i} = T_0(P_i/P_0)^{(\gamma_u-1)/\gamma_u} \tag{11}$$

$$P_{i-1}(V_{u,i-1} - V_{bb,i})^{\gamma_u} = P_i V_{u,i}^{\gamma_u} \tag{12}$$

$$V_{u,i} = (V_0 - V_{b,i-1} - V_{bb,i}) \sqrt[\gamma_u]{P_{i-1}/P_i} \tag{13}$$

$$V_{b,i} = V_0 - V_{u,i} \tag{14}$$

where $T_{u,i}$ is the temperature of unburned gas in time i; $\rho_{u,i}$ is the unburned gas density in time i.

3. Experimental Details

Experimental Set-Up

Experiments involving a hydrogen explosion were conducted in a cylindrical vessel with an inner diameter and height of 247 mm and 411 mm, respectively (Figure 2). In each test, hydrogen with a purity of 99.99% was used; the ignition unit consisted of a high-frequency pulse igniter with a 220 V voltage and two electrodes, as depicted in the previous study [25]. Due to the high-temperature effects of hydrogen combustion, the pressure sensor was protected by water-cooled circulation systems, with a sampling rate of 50 kHz (CYG 1409, Kunshan Shuangqiao Sensors Measurement and Control Technology Co., Ltd., Kunshan, China) [41].
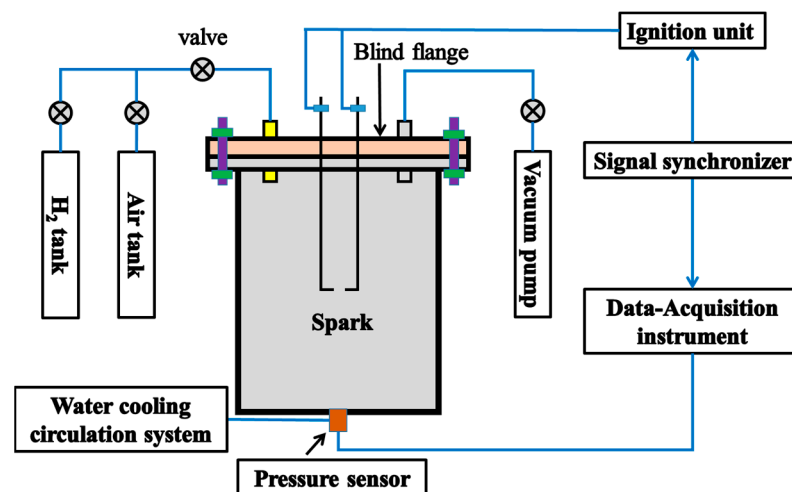

Figure 2. Experimental layout.

In the current tests, the vent was sealed by the blind flange, and the hydrogen and air were filled by the partial pressure method, respectively. The hydrogen–air mixture was mixed for about three minutes to ensure quiescence and homogeneity [41]. The spark ignition unit and the data acquisition equipment were controlled simultaneously by the synchronous controller. The ignition points were located at the center, as shown in Figure 2. Before the next test, the vessel was evacuated by a vacuum pump, then refilled with a fresh mixture, to ensure that the vessel was full of fresh air before starting the next test. All tests were conducted at 298 K and 1 atm.

4. Results and Discussion

4.1. Typical Pressure Profiles

Figure 3 shows a typical pressure–time history measured three times with a hydrogen concentration of 20 vol.%: the experimental results have good repeatability, and only a single pressure peak occurs during the hydrogen explosion.
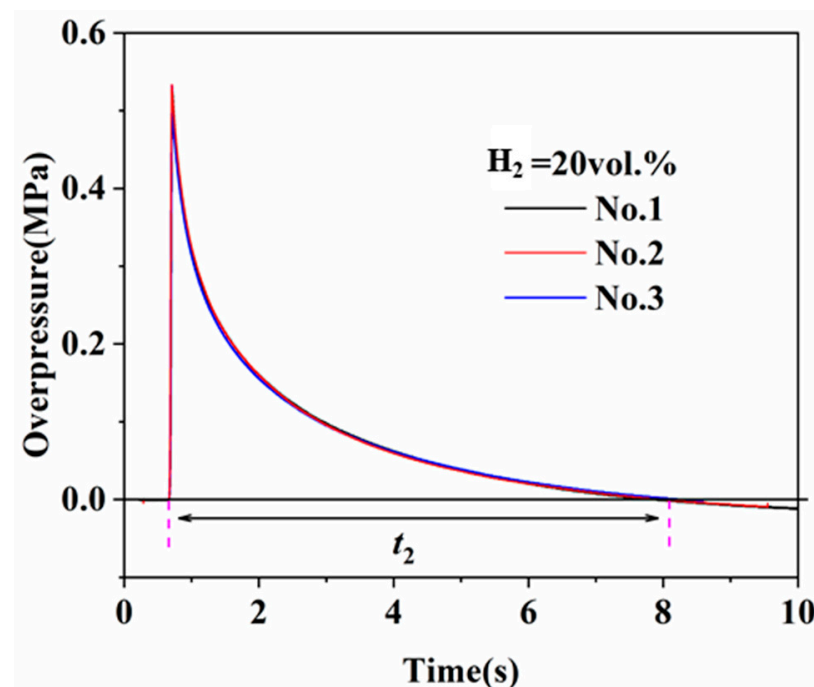

Figure 3. Pressure–time curves of three tests.

In this section, the effects of the vessel shape on the pressure profile with different hydrogen concentrations are shown in Figure 4. The spherical vessel was a 20 L vessel, which was cited by Zhang et al. [24]. The cylindrical vessel is shown in Figure 2. The result shows that the changes in peak pressure are the same with the increases of the hydrogen concentration in the spherical and cylindrical vessels, respectively. The peak pressure is maximized when the hydrogen concentration approaches 30 vol.%. In the case of low and high hydrogen concentrations, the hydrogen or oxygen in the confined space is insufficient to maintain a complete chemical reaction, respectively, causing a decrease in the explosion pressure [24]. After the pressure peak during the pressure–time curve, the pressure in the cylindrical vessel declines faster than that in a spherical vessel, due to the heat loss being larger in the cylindrical vessel, which results from the short distance between the ignition position and the sidewall in the cylindrical vessel. This causes the burned gas in the cylindrical vessel to make a contact with the wall faster than in the spherical vessel. In addition, Mitu et al. [42] also showed that in the case of a cylindrical vessel, higher heat losses and lower severity factors were presented in comparison with spherical vessels. Therefore, the overpressure decays fast in the cylindrical vessel.
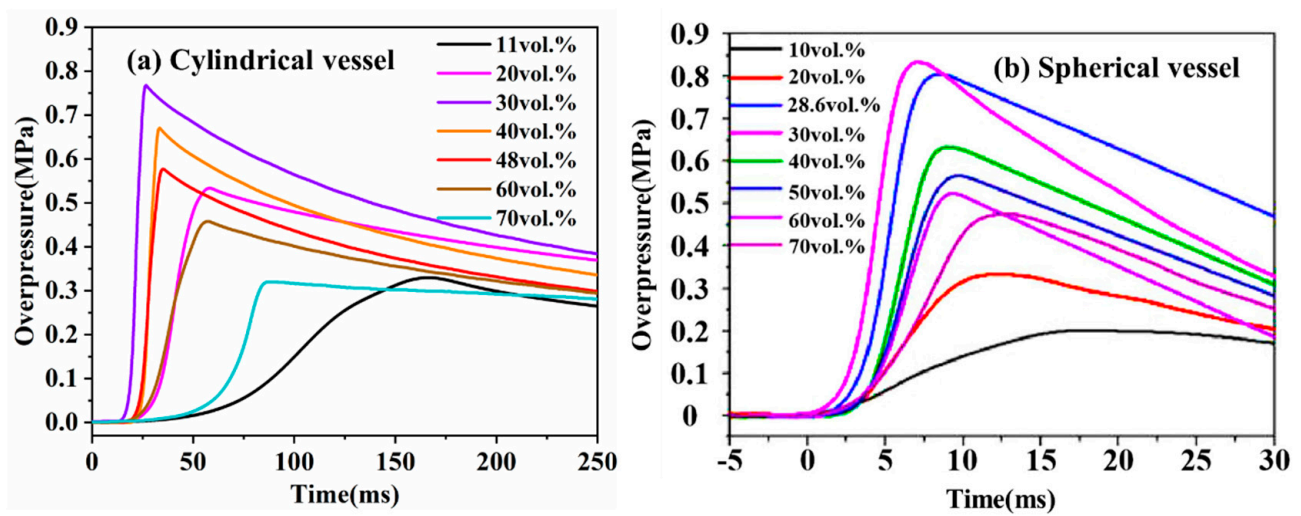
Figure 4. Pressure–time curves in different vessels: (**a**) current test, (**b**) Zhang et al. [24].

4.2. Validation of the Pressure Prediction Model

Based on the aforementioned derivation, the pressure histories calculated by the method were compared with the experimental results in different hydrogen concentrations in the current studies, as illustrated in Figure 5. The experimental conditions and parameters are listed in Table 2. The result shows that the hydrogen concentration has a significant effect on the temperature index and no effect on the pressure index. The temperature index increases with increasing hydrogen concentration. The P_e is always greater than P_{exp}, due to the heat loss by thermal conduction, convection, or radiation [43].
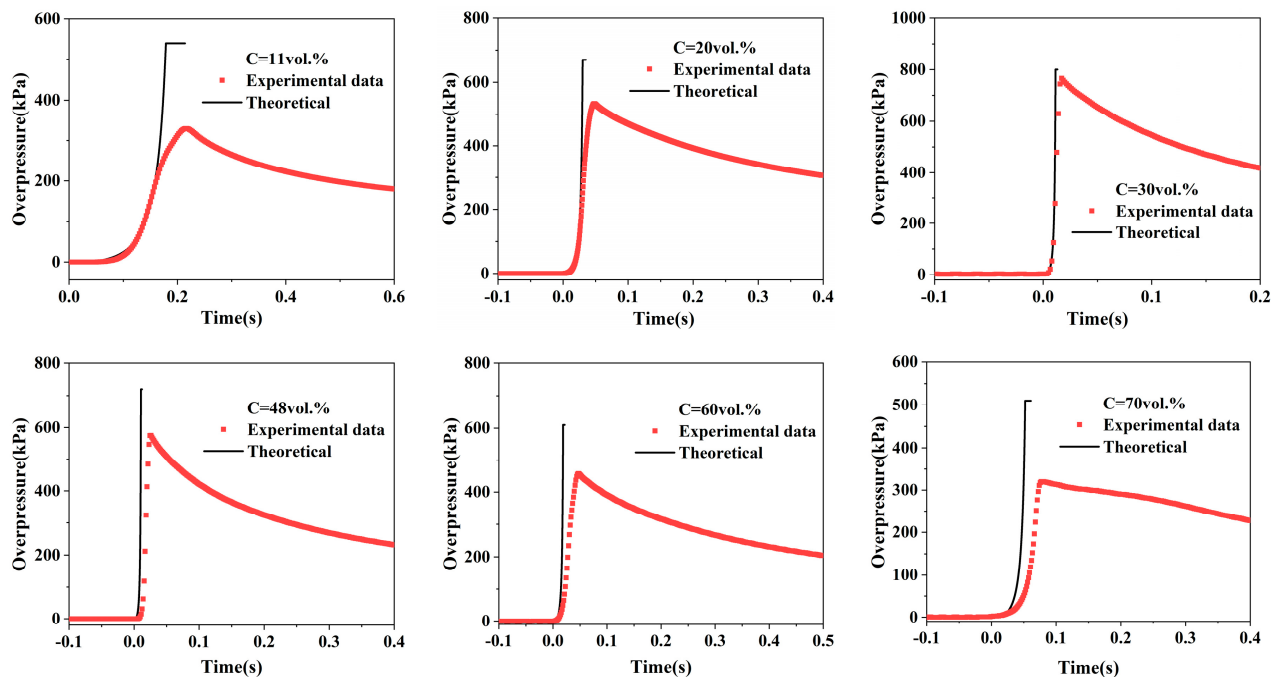

Figure 5. Pressure–time curves from experimental data and model prediction.

Table 2. Temperature index, pressure index, and maximum pressure with different hydrogen concentrations. P_e is defined as the adiabatic explosion pressure obtained from GASEQ software [44], P_{exp} is obtained by the current experiment, m and n are determined by Equations (8) and (9), respectively.

Concentration (vol.%)	m	n	P_e (kPa) [44]	P_{exp} (kPa)
11	1.52	0.43	547	340
20	1.53	0.43	679	530
30	1.54	0.43	811	770
40	1.56	0.43	780	760
48	1.57	0.43	730	576
60	1.60	0.44	628	460
70	1.66	0.44	527	320

Figure 5 shows the effect of the hydrogen concentration on the pressure histories. The pressure–time curves calculated in the current model agree with the experimental data. In the initial stage of the explosion, the curves obtained through the theory and experiments are almost the same; this is because the flame front does not touch the vessel wall, so the heat loss is less, which is mainly caused by thermal radiation. As combustion propagates, the difference between the theoretical and the experimental values increases with time, which results from the heat loss by thermal conduction, convection, or radiation in the vicinity of the vessel wall. In addition, the difference first decreases to the minimum at a hydrogen concentration of 30 vol.% and then increases with increasing hydrogen concentration. This is because the laminar burning velocity is very large when the hydrogen concentration is close to the stoichiometric concentration [40,45], resulting in a reduction in the chemical reaction time and an increase in the rate of heat release during the period of rising pressure. At the upper and lower explosive limits of the hydrogen concentration, a large difference arises because the incomplete combustion of the hydrogen–air mixture reduces the laminar burning velocity and heat release, increasing the duration of the pressure rise, which results in an increased loss of heat; therefore, the profiles obtained by the model are larger than those measured.

Figure 5 indicates that the experimental pressure peak is always lower than the calculated pressure, which is due to heat loss and incomplete combustion as discussed above. The same result was obtained by Wang et al. [43] and Jo et al. [46]. When the hydrogen concentration is close to the stoichiometric concentration, the burning velocity is very fast; the pressure peak measured is the maximum at a hydrogen concentration of 30 vol.%, which is consistent with the results obtained using the current model. The reason for this can be explained by the fact that the rate of release of energy of the hydrogen combustion is much greater than the rate of heat loss through the wall; therefore, the heat loss has little effect on the peak pressure; however, in the case of rich and lean concentrations of fuel, the difference in the pressure peak between the experimental and theoretical data increases, because the incomplete combustion of the gas mixture results in a relatively small amount of heat released; when the burnt gas makes contact with the cold wall of the vessel, the heat losses become even stronger (enhanced to some extent by free convection) [47]. Therefore, the pressure peak measured by the experiment is very low compared with the calculated pressure, which is also similar to the result observed for the methane–air mixtures [48].

4.3. Analysis of the Predictive Model

The accuracy of the computer model can be verified by comparing the results obtained from previous experimental data of hydrogen and methane in different-sized vessels, respectively. The pressure profiles measured were compared with the predicted results (Figures 6 and 7).
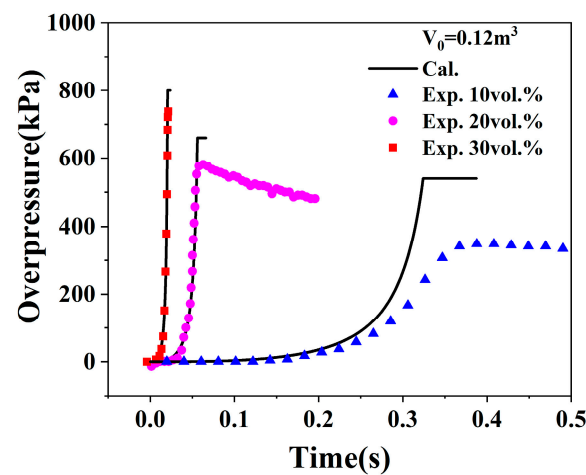
Figure 6. Pressure evolution vs. hydrogen concentrations. The black line represents data calculated using the model and the symbols denote experimental results (T_0 = 298 K and P_0 = 1 atm) [46].
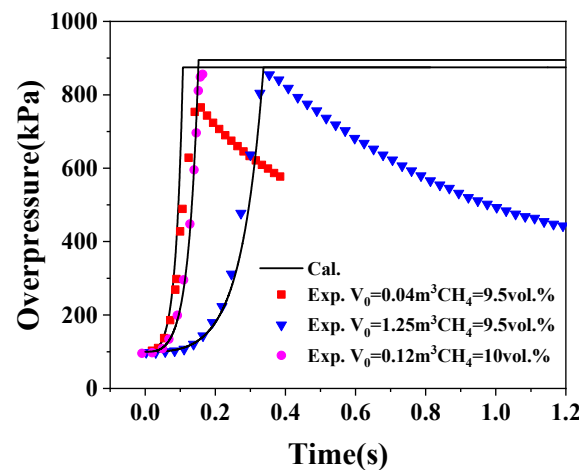

Figure 7. Pressure–time curves of different vessels. The black line represents data calculated using the method and the symbols denote experimental results (V_0 = 0.04 m^3 and 1.25 m^3 [47]; V_0 = 0.12 m^3 [48]).

As can be seen in Figure 6, the pressure curves calculated by the current model as a function of hydrogen concentrations are in good agreement with the experimental results for V_0 = 0.12 m^3. However, in the case of the final stage, when the hydrogen concentration is 10 vol.%, the pressure measured in the experiment is lower because of the substantial heat loss through the vessel wall and the incomplete combustion, respectively. The result is akin to the current experimental data, as mentioned above. Figure 7 implies that the effect of vessel size on the pressure histories obtained by the prediction model was compared to the experimental data of the methane explosion, which come from work by Kobiera et al. [47] and Cashdollar et al. [48]. The laminar flame speed of CH_4–air mixtures was calculated by GASEQ software [44]. The results show that the predicted pressure value is in reasonable agreement with the experimental data in the three vessels. As the size of the vessel decreases, the volume of the flammable gas reduces, leading to the decrease in the heat released by the combustion, the distance between the ignition point and the vessel wall decreases, and the specific surface area increases, which causes an increase in the heat loss through the vessel wall. Therefore, the peak pressure decreases with increasing vessel volume. By comparing the above data, this observation indicates that the proposed method could be used to predict the pressure profiles of hydrogen and methane explosions.

4.4. Analysis of Explosion Parameters

The maximum rate of change in pressure and the explosion index are the most important safety parameters to assess explosion hazards and design vessels capable of surviving the explosion [25,49]. This deflagration index is calculated using Equation (1), which is key to estimating vent areas for the explosion venting design during a catastrophic accident. To investigate the explosion behavior, the evolution of pressure rise rate was obtained by differentiating the pressure–time curves, as shown in Figure 8, and the explosion parameters (maximum pressure P_{max} and corresponding time t_1, positive pressure duration t_2 in Figure 3, $(dP/dt)_{max}$, and corresponding time $t_{1'}$) are defined in the present study.
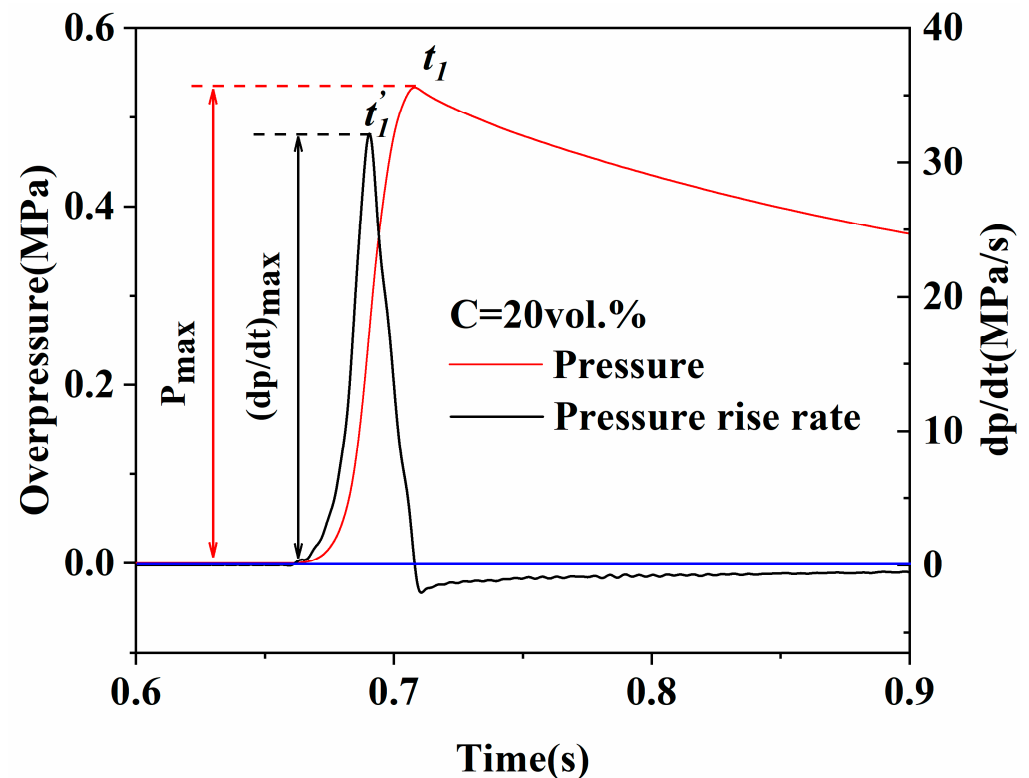

Figure 8. Typical pressure and dP/dt time profiles.

The experimental deflagration index (K_G) and pressure peak versus the hydrogen concentration are shown in Figure 9: the deflagration index and pressure peak first increase, then decrease with the increase in the hydrogen concentration, revealing its maximum value at the hydrogen concentration of about 30 vol.% [50]. This is due to the fact that, when the hydrogen concentration is close to the stoichiometric concentration, the chemical reaction is the fastest, which increases the amount and rate of heat release, resulting in the maximum pressure rise rate and pressure peak; in the case of the hydrogen flammable upper or lower limit, the incomplete burning leads to the decrease in the heat release and combustion velocity, causing the increase in combustion time and heat loss; therefore, the pressure rise rate and pressure peak decrease further, the further the hydrogen–air mixture is from stoichiometric. In addition, the result is also attributed to the fact that the time (t_1) corresponding to P_{max}, and the time to $(dP/dt)_{max}$ are the shortest at a hydrogen concentration of 30 vol.% (Figure 11), indicating that the combustion is the fastest.
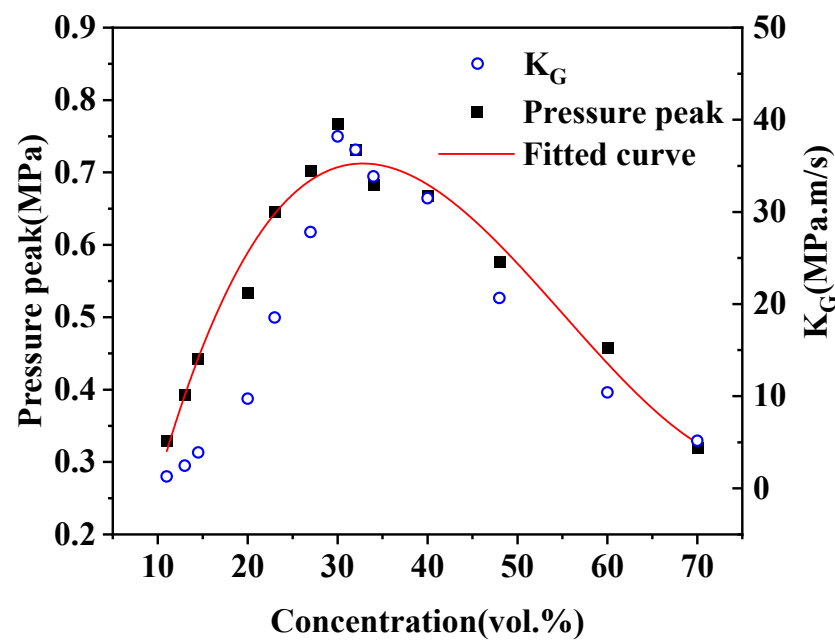
Figure 9. Peak pressure and deflagration index vs. the hydrogen concentration.

Table 3 lists the maximum pressure peak, maximum pressure rise rate, and deflagration index for the stoichiometric hydrogen–air mixture in different vessels. The value of P_{max} measured during the experiment is lower than that predicted using the theoretical calculation [44], which is due to the heat loss through thermal conduction, convection, or radiation [43]. In addition, large discrepancies between the three parameters are observed, which arise from the significant effects of the aspect ratio and specific surface area of the cylindrical vessel on P_{max} and $(dP/dt)_{max}$. Meanwhile, Wang et al. [51] suggested that both P_{max} and $(dP/dt)_{max}$ decrease with the increases in aspect ratio and specific surface area [43,49]. The results of Razus et al. [52] showed that K_G increases with vessel volume, indicating that the effects of the vessel size and shape on the deflagration parameters are irregular.

Table 3. Explosion parameters of hydrogen stoichiometric concentration in various vessels.

Shape	Volume (L)	P_{max} (MPa)	$(dP/dt)_{max}$ (MPa/s)	K_G (MPa·m/s)	P_e (MPa)	Ref.
Sphere	5	0.740	321	54.9		[53]
Cylinder	5	0.755	126	21.5		[54]
Sphere	20	0.695	115	31.2	0.801	[55]
Cylinder	7.3	0.785	213	41.3		[43]
Cylinder	120	0.710	223	110		[56]
Cylinder	20	0.767	141.5	38.4		This study

Regarding the explosion damage effect, overpressure and impulse are the two most important and dangerous factors, resulting in personal injury and structural damage [57]. The impulse value was calculated by integrating the overpressure–time curves within the time range of the positive pressure duration (t_2).

$$I = \int_0^{t2} p(t)dt \tag{15}$$

Figure 10 presents the maximum overpressure (P_{max}) and impulse for various hydrogen concentrations in a cylindrical vessel; P_{max} first increases, and then decreases with increasing hydrogen concentration, and P_{max} reaches a maximum value when the hydrogen concentration is about 30 vol.%, which is in line with that measured by Zhang et al. [24,58].

This result is discussed above (Figure 9); however, the maximum impulse appears when the hydrogen concentration is about 20 vol.%, and the impulse measured at hydrogen fuel-rich mixture exceeds that at a hydrogen fuel-lean concentration. This is due to the fact that the impulse is related to the pressure peak and positive pressure duration, which is explained by Equation (15). As illustrated in Figure 11, the time (t_1) corresponding to P_{max}, the time (t_2) corresponding to $(dP/dt)_{max}$, and positive pressure duration time t_2 decrease, and reach their minimum value at a hydrogen concentration of 30 vol.%, and then increase with the hydrogen concentration. In the case of the hydrogen fuel-rich concentration, all the time parameters are smaller than those of fuel-lean concentrations. Meanwhile, the P_{max} value is almost symmetrical concerning the hydrogen concentration of 30 vol.%; therefore, the impulse is greater when the hydrogen concentration is lean.
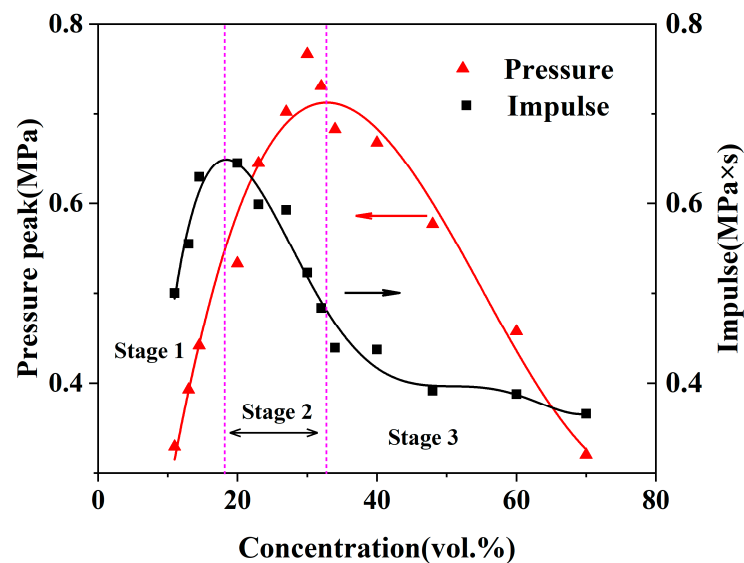
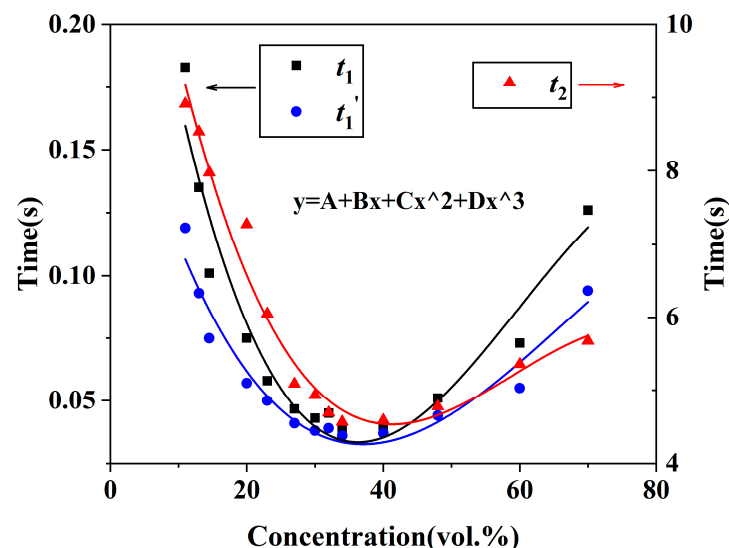**Figure 10.** Overpressure and impulse vs. the hydrogen concentration.

Figure 11. Time parameters vs. the hydrogen concentration.

In addition, according to the fitted curve in Figure 10, the pressure and impulse are divided into three stages: in the first stage, the impulse and pressure increase with the hydrogen concentration, and then the impulse reaches the maximum corresponding to the hydrogen concentration of 18 vol.%. This is due to the fact that the impulse depends on the pressure and the time (Equation (15)). At a low concentration of hydrogen, the

positive pressure duration (t_2) decreases; as the combustion velocity is much slower, a slower reduction in the time t_2 occurs; however, the pressure increases with increasing hydrogen concentration; therefore, the impulse increases to the maximum. In the second stage, as the hydrogen concentration increases, the hydrogen concentration is close to the stoichiometric concentration; the rate of combustion is faster, resulting in a rapid decrease in the time t_2, as shown in Figure 11. The pressure peaks increase slowly, which leads to a decrease in the impulse value, and the pressure peak reaches the maximum when the hydrogen concentration is about 34 vol.%. In the last stage, the pressure and impulse decrease with increasing hydrogen concentration. This can be explained by the reason that the incomplete combustion leads to a slow increase in positive pressure time t_2, and is less than the value obtained at lower concentrations (Figure 11), and the pressure with increasing concentration. Furthermore, when the hydrogen concentration is between 18 vol.% and 34 vol.%, the harm caused to personnel and the structural damage caused by a hydrogen explosion arise mainly from the impulse and the pressure peak, which leads to a more severely destructive effect. Therefore, to assess the structural damage caused by a gas explosion, both the overpressure peak and the impulse should be considered.

As can be seen in Figure 11, the changes in the time parameters with the hydrogen concentration are similar; the function $y = A + Bx + Cx^2 + Dx^3$ fits the relationship, where A, B, C, and D are coefficients. The results show that the time first decreases, then increases with the increase in the hydrogen concentration, and the minimum time occurs at a hydrogen concentration of around 34 vol.% from the fitted curves, indicating that the rate of combustion is very fast. Meanwhile, the time obtained in the fuel-rich concentration is greater than that at a fuel-lean concentration, revealing that the rate of combustion of the hydrogen–air mixture at fuel-rich concentrations is obviously higher than that at fuel-lean concentrations. As is discussed above, the impulse from a hydrogen explosion is not only related to the overpressure but also the time; therefore, the analysis of the destructive effect of a hydrogen explosion on personnel and structures warrants consideration of the time parameter of the hydrogen explosion when trying to minimize the damage caused by the impulse.

5. Conclusions

In this study, the theoretical model that considers the burnout rate was established by using the distributed computing method as a simple tool for calculating gaseous combustion pressure profiles in a closed vessel. The experimental data for the hydrogen–air mixture were obtained in a cylindrical vessel to investigate the impulse, pressure peak, duration, and deflagration index.

The pressure profiles predicted by the current model agree with the experimental results; the pressure peak difference between experiment and theory first decreases to the minimum at a hydrogen concentration of 30 vol.%. The pressure peak and pressure rise rate increase and then decrease as the hydrogen concentration increases. The deflagration parameters ($P_{\max}$, $(dP/dt)_{max}$, and K_G) depend on the aspect ratio and specific surface area.

The maximum value of $P_{\max}$ and impulse occur at hydrogen concentrations of 34 vol.% and 18 vol.%, respectively. When the hydrogen concentration is in the range of 34 vol.% and 18 vol.%, both the overpressure and the impulse lead to the greatest explosion damage effect. In the case of a fuel-lean concentration, the impulse and time parameters exceed the value obtained at fuel-rich concentrations.

Conflicts of Interest: The authors declare no conflict of interest.

References

1. Gong, L.; Duan, Q.; Sun, J.; Molkov, V. Similitude analysis and critical conditions for spontaneous ignition of hydrogen release into the atmosphere through a tube. *Fuel* **2019**, *245*, 413–419. [CrossRef]
2. Zhang, Y.; Cheng, Y.; Su, J.; Wang, W.; Han, T.; Tan, Y.; Cao, W. Experimental investigation on the near detonation limits of propane/hydrogen/oxygen mixtures in a rectangular tube. *Int. J. Hydrog. Energy* **2020**, *45*, 1107–1113.
3. Shen, X.; Zhang, C.; Xiu, G.; Zhu, H. Evolution of premixed stoichiometric hydrogen/air flame in a closed duct. *Energy* **2019**, *176*, 265–271. [CrossRef]
4. Sarli, V.D.; Benedetto, A.D. Sensitivity to the Presence of the Combustion Submodel for Large Eddy Simulation of Transient Premixed Flame–Vortex Interactions. *Ind. Eng. Chem. Res.* **2012**, *51*, 7704–7712. [CrossRef]
5. Li, Y.; Bi, M.; Li, B.; Zhou, Y.; Huang, L.; Gao, W. Explosion hazard evaluation of renewable hydrogen/ammonia/air fuels. *Energy* **2018**, *159*, 252–263. [CrossRef]
6. Bjerketvedt, D.; Bakke, J.R.; Wingerden, K.V. Gas explosion handbook. *J. Hazard. Mater.* **1997**, *52*, 1–150. [CrossRef]
7. Taveau, J. Explosion of fixed roof atmospheric storage tanks, part 1: Background and review of case histories. *Process Saf. Prog.* **2011**, *30*, 381–392. [CrossRef]
8. Sun, X.; Lu, S. Effect of orifice plate on the transmission mechanism of a detonation wave in hydrogen-oxygen mixtures. *Int. J. Hydrog. Energy* **2020**, *45*, 12593–12603. [CrossRef]
9. Rui, S.; Li, Q.; Guo, J.; Sun, X. Experimental and numerical study on the effect of low vent burst pressure on vented methane-air deflagrations. *Process Saf. Environ.* **2021**, *146*, 35–42. [CrossRef]
10. Sun, X.; Lu, S. On the mechanisms of flame propagation in methane-air mixtures with concentration gradient. *Energy* **2020**, *202*, 117782. [CrossRef]
11. Bradley, D.; Mitcheson, A. Mathematical solutions for explosions in spherical vessels. *Combust. Flame* **1976**, *26*, 201–217. [CrossRef]
12. Jo, Y.D.; Crowl, D.A. Flame Growth Model for Confined Gas Explosion. *Process Saf. Prog.* **2010**, *28*, 141–146. [CrossRef]
13. Walsh, B.P.; Snodgrass, R.E.; Black, W.Z. Thermodynamic model for gas explosions in vented and non-vented enclosures. *Combust. Sci. Technol.* **2016**, *189*, 366–394. [CrossRef]
14. Rota, R.; Canu, P.; Carrà, S.; Morbidelli, M. Vented gas deflagration modeling: A simplified approach. *Combust. Flame* **1991**, *85*, 319–330. [CrossRef]
15. Canu, P.; Rota, R.; Carrà, S.; Morbidelli, M. Vented gas deflagrations a detailed mathematical model tuned on a large set of experimental data. *Combust. Flame* **1990**, *80*, 49–64. [CrossRef]
16. Thomas, G.O.; Oakley, G.L. Overpressure development during the combustion of a hydrogen–air mixture partial filling a confined space. *Process Saf. Env.* **2010**, *88*, 24–27. [CrossRef]
17. Dahoe, A.E. Laminar burning velocities of hydrogen–air mixtures from closed vessel gas explosions. *J. Loss Prev. Proc.* **2005**, *18*, 152–166. [CrossRef]
18. Sun, X.; Yan, C.; Yan, Y.; Mi, X.; Lee, J.H.S.; Dick Ng, H. Critical tube diameter for quasi-detonations. *Combust. Flame* **2022**, *244*, 112280. [CrossRef]
19. Sun, X.; Li, Q.; Xu, M.; Wang, L.; Guo, J.; Lu, S. Experimental study on the detonation propagation behaviors through a small-bore orifice plate in hydrogen-air mixtures. *Int. J. Hydrog. Energy* **2019**, *44*, 15523–15535. [CrossRef]
20. Sun, X.; Li, Q.; Li, C.; Lu, S. Detonation propagation characteristics for CH_4-$2H_2$-$3O_2$ mixtures in a tube filled with orifice plates. *Int. J. Hydrog. Energy* **2019**, *44*, 7616–7627. [CrossRef]
21. Sun, X.; Lu, S. Effect of obstacle thickness on the propagation mechanisms of a detonation wave. *Energy* **2020**, *198*, 117186. [CrossRef]
22. Cao, W.; Li, W.; Yu, S.; Zhang, Y.; Shu, C.; Liu, Y.; Luo, J.; Bu, L.; Tan, Y. Explosion venting hazards of temperature effects and pressure characteristics for premixed hydrogen-air mixtures in a spherical container. *Fuel* **2021**, *290*, 120034. [CrossRef]
23. Cao, W.; Li, W.; Zhang, L.; Chen, J.; Yu, S.; Zhou, Z.; Zhang, Y.; Shen, X.; Tan, Y. Flame characteristics of premixed H_2-air mixtures explosion venting in a spherical container through a duct. *Int. J. Hydrog. Energy* **2021**, *46*, 26693–26707. [CrossRef]
24. Zhang, Y.; Cao, W.; Shu, C.; Zhao, M.; Yu, C.; Xie, Z.; Liang, J.; Song, Z.; Cao, X. Dynamic hazard evaluation of explosion severity for premixed hydrogen–air mixtures in a spherical pressure vessel. *Fuel* **2020**, *261*, 116433. [CrossRef]
25. Xing, H.; Qiu, Y.; Sun, S.; Wang, M.; Li, B.; Xie, L. Visualization of explosion characteristics of methane-air mixtures with different ignition positions and vent areas in a large-scale venting chamber. *Fuel* **2020**, *279*, 118380. [CrossRef]
26. Cao, W.; Qin, Q.; Cao, W.; Lan, Y.; Chen, T.; Xu, S.; Cao, X. Experimental and numerical studies on the explosion severities of coal dust/air mixtures in a 20-L spherical vessel. *Powder Technol.* **2017**, *310*, 17–23. [CrossRef]
27. Zhang, C.; Li, Y.; Sun, X.; Chen, X.; Huang, C.; Yuan, B. Investigation on the characteristics of vented stoichiometric methane-air explosion: Effect of ignition positions and obstacles. *Fuel* **2022**, *329*, 125417. [CrossRef]
28. Razus, D.; Movileanua, C.; Oancea, D. The rate of pressure rise of gaseous propylene–air explosions in spherical and cylindrical enclosures. *J. Hazard. Mater.* **2007**, *139*, 1–8. [CrossRef]
29. *NFPA68*; Standard on Explosion Protection by Deflagration Venting. National Fire Protection Association: Quincy, MA, USA, 2007.
30. Sun, Z.; Li, G. Turbulence influence on explosion characteristics of stoichiometric and rich hydrogen/air mixtures in a spherical closed vessel. *Energy Convers. Manag.* **2017**, *149*, 526–535. [CrossRef]

31. Tang, C.; Huang, Z.; Jin, C.; He, J.; Wang, J.; Wang, X.; Miao, H. Explosion characteristics of hydrogen–nitrogen–air mixtures at elevated pressures and temperatures. *Int. J. Hydrog. Energy* **2009**, *34*, 554–561. [CrossRef]

32. van Wingerden, K.; Slavesen, H.; Perbal, R. Simulation of an accidental vapor cloud explosion. *Process Saf. Prog.* **1995**, *14*, 173–181. [CrossRef]

33. Li, J.; Hao, H. Numerical and analytical prediction of pressure and impulse from vented gas explosion in large cylindrical tanks. *Process Saf. Environ.* **2019**, *127*, 226–244. [CrossRef]

34. Ferradás, E.G.; Alonso, F.D.; Miñarro, M.D.; Aznar, A.M.; Gimeno, J.R.; Pérez, J.F.S. Consequence analysis by means of characteristic curves to determine the damage to humans from bursting spherical vessels. *Process Saf. Environ.* **2008**, *86*, 121–129. [CrossRef]

35. Alonso, F.D.; Ferradas, E.G.; Perez, J.F.S.; Aznar, A.M.; Gimeno, J.R.; Alonso, J.M. Characteristic overpressure-impulse-distance curves for vapour cloud explosions using the TNO Multi-Energy model. *J. Hazard. Mater.* **2006**, *137*, 734–741. [CrossRef] [PubMed]

36. Grossel, S.S. Loss prevention in the process industries. *J. Loss Prev. Proc.* **1997**, *10*, 285. [CrossRef]

37. Faghih, M.; Gou, X.; Chen, Z. The explosion characteristics of methane, hydrogen and their mixtures: A computational study. *J. Loss Prev. Proc.* **2016**, *40*, 131–138. [CrossRef]

38. Xiao, H.; Duan, Q.; Sun, J. Premixed flame propagation in hydrogen explosions. *Renew. Sustain. Energy Rev.* **2018**, *81*, 1988–2001. [CrossRef]

39. Poinsot, T.; Veynante, D. *Theoretical and Numerical Combustion*; RT Edwards: Morningside, QLD, Australia, 2005.

40. Biennial Report on Hydrogen Safety (Version 1.2). 2007. Available online: http://www.hysafe.org/BRHS (accessed on 11 October 2022).

41. Qiu, Y.; Xing, H.; Sun, S.; Wang, M.; Li, B.; Xie, L. Experimental study of the effects of vent area and ignition position on internal and external pressure characteristics of venting explosion. *Fuel* **2021**, *300*, 120935. [CrossRef]

42. Mitu, M.; Giurcan, V.; Razus, D.; Prodan, M.; Oancea, D. Propagation indices of methane-air explosions in closed vessels. *J. Loss Prev. Proc.* **2017**, *47*, 110–119. [CrossRef]

43. Wang, L.; Ma, H.; Shen, Z.; Chen, D. The influence of an orifice plate on the explosion characteristics of hydrogen-methane-air mixtures in a closed vessel. *Fuel* **2019**, *256*, 115908. [CrossRef]

44. Morley, C. Gaseq a Chemical Equilibrium Program for Windows. 2005. Available online: http://www.gaseq.co.uk (accessed on 11 October 2022).

45. Okafor, E.C.; Hayakawa, A.; Nagano, Y.; Kitagawa, T. Effects of hydrogen concentration on premixed laminar flames of hydrogen–methane–air. *Int. J. Hydrog. Energy* **2014**, *39*, 2409–2417. [CrossRef]

46. Jo, Y.D.; Crowl, D.A. Explosion characteristics of hydrogen-air mixtures in a spherical vessel. *Process Saf. Prog.* **2010**, *29*, 216–223. [CrossRef]

47. Kobiera, A.; Kindracki, J.; Zydak, P.; Wolanski, P. A new phenomenological model of gas explosion based on characteristics of flame surface. *J. Loss Prev. Proc.* **2007**, *20*, 271–280. [CrossRef]

48. Cashdollar, K.L.; Zlochower, I.A.; Green, G.M.; Thomas, R.A.; Hertzberg, M. Flammability of methane, propane, and hydrogen gases. *J. Loss Prev. Proc.* **2000**, *13*, 327–340. [CrossRef]

49. Mitu, M.; Giurcan, V.; Razus, D.; Oancea, D. Influence of initial pressure and vessel's geometry on deflagration of stoichiometric methane–air mixture in small-scale closed vessels. *Energy Fuels* **2020**, *34*, 3828–3835. [CrossRef]

50. Cao, W.; Liu, Y.; Chen, R.; Li, W.; Zhang, Y.; Xu, S.; Cao, X.; Huang, Q.; Tan, Y. Pressure release characteristics of premixed hydrogen-air mixtures in an explosion venting device with a duct. *Int. J. Hydrog. Energy* **2021**, *46*, 8810–8819. [CrossRef]

51. Wang, L.; Ma, H.; Shen, Z. Explosion characteristics of hydrogen-air mixtures diluted with inert gases at sub-atmospheric pressures. *Int. J. Hydrog. Energy* **2019**, *44*, 22527–22536. [CrossRef]

52. Razus, D.; Movileanu, C.; Brinzea, V.; Oancea, D. Closed vessel combustion of propylene–air mixtures in the presence of exhaust gas. *Fuel* **2007**, *86*, 1865–1872. [CrossRef]

53. Bartknecht, W. *Explosions: Course, Prevention, Protection*; Springer: Berlin, Germany, 1981.

54. Salzano, E.; Cammarota, F.; Di Benedetto, A.; Di Sarli, V. Explosion behavior of hydrogen–methane/air mixtures. *J. Loss Prev. Proc.* **2012**, *25*, 443–447. [CrossRef]

55. Ma, Q.; Zhang, Q.; Chen, J.; Huang, Y.; Shi, Y. Effects of hydrogen on combustion characteristics of methane in air. *Int. J. Hydrog. Energy* **2014**, *39*, 11291–11298. [CrossRef]

56. Cashdollar, K.L.; Zlochower, I.A. Explosion temperatures and pressures of metals and other elemental dust clouds. *J. Loss Prev. Proc.* **2007**, *20*, 337–348. [CrossRef]

57. Melani, L.; Sochet, I.; Rocourt, X.; Jallais, S.; Josas, F. In Review of methods for estimating the overpressure and impulse resulting from a hydrogen explosion in a confined/obstructed volume. In Proceedings of the 3rd International Conference on Hydrogen Safety, Ajjacio, France, 16–18 September 2009; pp. 16–18.

58. Zhang, Y.; Chen, R.; Zhao, M.; Luo, J.; Feng, W.; Fan, W.; Tan, Y.; Cao, W.; Shu, C.; Yu, C. Hazard evaluation of explosion venting behaviours for premixed hydrogen-air fuels with different bursting pressures. *Fuel* **2020**, *268*, 117313. [CrossRef]